



## Synthesis and biological evaluation of a series of podophyllotoxins derivatives as a class of potent antitubulin agents

Yingqian Liu<sup>a</sup>, Dongfeng Wei<sup>b</sup>, Yonglong Zhao<sup>a</sup>, Weidong Cheng<sup>b</sup>, Yan Lu<sup>a</sup>, Yaqiong Ma<sup>a</sup>, Xin Li<sup>c</sup>, Chao Han<sup>a</sup>, Yanxia Wei<sup>b</sup>, Huiming Cao<sup>a</sup>, Chunyan Zhao<sup>a,\*</sup>

<sup>a</sup>School of Pharmacy, Lanzhou University, Lanzhou 730000, China

<sup>b</sup>School of Basic Medicine, Lanzhou University, Lanzhou 730000, China

<sup>c</sup>College of Food and Bioengineering, Henan University of Science and Technology, Luoyang 471003, China

### ARTICLE INFO

#### Article history:

Received 26 July 2012

Revised 4 September 2012

Accepted 6 September 2012

Available online 13 September 2012

#### Keywords:

Podophyllotoxin derivatives

Microtubules

Antiproliferative

Docking

Molecular dynamic

### ABSTRACT

A series of eight novel podophyllotoxin derivatives were designed, synthesized and evaluated for biological activities. The antiproliferative activities were tested against a panel of human cancer cell lines (K562, SGC, HeLa and HepG) and the inhibition of tubulin polymerization was also evaluated. Compound **8e** displayed significant antiproliferative activities for all four cell lines and strong levels of tubulin polymerization inhibition effect. Combined with cell apoptosis and cell cycle analysis, it demonstrated that compound **3e** that effectively interfere with tubulin dynamics prevent mitosis in cancer cells, leading to cell cycle arrest and, eventually dose dependent apoptosis. All experimental measurements were also supported by molecular docking simulations of colchicine binding site, which revealed the governing forces for the binding behavior and a good relationship with anti-tubulin activity and antiproliferative activities. The synthesis and biological studies provided an interesting new class of antitubulin agents for development of lead compounds and also a direction for further structure modification to obtain more potent anti-cancer drugs.

© 2012 Elsevier Ltd. All rights reserved.

### 1. Introduction

Microtubules (MTs), constructed from a heterodimer of two highly homologous proteins known as  $\alpha$ - and  $\beta$ -tubulin, are ubiquitous, essential cytoskeletal polymers in all eukaryotic cells.<sup>1</sup> The microtubule system plays a crucial role in a broad range of cellular processes, including the mitosis, exocytosis, maintenance of cellular morphology and active transport of cellular components throughout the cytoplasm.<sup>2,3</sup> Especially, it has an essential role in cell division because microtubules are the key component for formation of the mitotic spindle apparatus, providing the mechanical force required for chromosome separation during mitosis.<sup>4</sup> It made microtubules an attractive and successful target to treat many types of malignancies. In this regard, tubulin, as the main component of the microtubules represents an important target to anti-cancer therapy. The discovery for new compounds with stabilize or destabilize microtubules activity is considered one of the most promising ways for treating cancer disease.<sup>5</sup>

Microtubules are a dynamic cellular compartment in both neoplastic and normal cells. The dynamicity is characterized by the continuous turnover of  $\alpha$ , $\beta$ -tubulin heterodimers in the polymeric microtubules.<sup>6</sup> Generally, most of the biological functions of MTs

are strongly associated with their stability, which is often regulated by the interaction of various small molecules and tubulin proteins. The dynamics interference of tubulin induced by some natural or synthetic substances has been proven to be clinically useful for designing anticancer agents.<sup>7,8</sup> The application of polymerization or depolymerization agents can normalize abnormal tumor vasculature and leads to more efficient need to develop new tubulin-targeted compounds for chemotherapy.<sup>9–11</sup>

Now there were a large number of chemically different tubulin binding agents targeting the vascular system of tumors and these exogenous ligands did dramatic effects on microtubules, often interacting directly with tubulin to either stabilize (such as paclitaxel)<sup>12,13</sup> or destabilize microtubules (such as colchicine).<sup>14,15</sup> These ligands can disrupt the dynamics of polymerization for microtubules involved in cell division.<sup>16</sup> The specific effects on the microtubules dynamics were complex and depended on the different binding site, including taxol site, vinblastine site and colchicine sites.<sup>17</sup> For example, colchicine generally showed potent inhibition effects of polymerization by blocking colchicine's binding site and rapidly shutting down existing tumor vasculature.<sup>13,18</sup> And there is conclusive evidence that microtubule disruption affected by colchicine caused cell cycle arrest mainly at the G2/M phase, and subsequently induced apoptosis, a cell suicide mechanism.<sup>19</sup>

Indeed, the findings that some tubulin binding agents targeting the vascular system of tumors has extended their use.<sup>20–22</sup> In this

\* Corresponding author. Tel.: +86 931 8915686; fax: +86 931 8915685.

E-mail address: [zhaochy07@lzu.edu.cn](mailto:zhaochy07@lzu.edu.cn) (C. Zhao).

regard, podophyllotoxin behaves in the same way as colchicine, the binding of which to tubulin results in partial unfolding of the secondary structure of  $\beta$ -tubulin at the carboxy terminus and prevents polymerization.<sup>23,24</sup> Podophyllotoxins (**1**), as naturally aryl tetralin lignan which has been found in a variety of plants, including *Podophyllum peltatum* and *Juniperus Sabina*<sup>25,26</sup> are generally believed to be an effect agent which is able to inhibit tubulin assembly by binding with its colchicine domain. Furthermore, the microtubule disruption affected by podophyllotoxins leads to cell cycle arrest and, eventually dose dependent apoptosis caused cell cycle arrest.<sup>27,28</sup> For now, research has identified podophyllotoxin and their derivatives as clinically useful drugs against various cancers, including small cell lung cancer, testicular carcinoma, lymphoma, and Kaposi's sarcoma.<sup>29,30</sup> Considering the cyclolignanskeleton, nearly every ring of the molecule (A to E) has been modified. Modification of the podophyllotoxin structure has revealed structural features critical for anticancer activity: (a) the 4 $\beta$ -configuration is essential with various substituents at C(4); (b) the trans-lactone D ring with 2 $\alpha$ ,3 $\beta$ -configuration is very important; (c) the dioxolane A ring is optimal; and (d) the free rotation of ring E is required. It was demonstrated that an important role of various C-4 substitutions in the activity profiles of podophyllotoxin analogues and the feasibility of optimizing this compound class through rational C-4 modification.<sup>31–34</sup>

Therefore, we introduced the sulfonylamidine groups to podophyllotoxin via a Cu-catalyzed reaction in the present study. All the synthesized podophyllotoxin derivatives were then screened for anticancer activity against a panel of four human cancer cell lines. Biological evaluations including cell cycle, cell apoptosis analysis and the direct assay for inhibition of polymerization were constructed to probe the interference with tubulin dynamics. All experimental measurements were also supported by computational research including docking and molecular dynamics, indicated that the podophyllotoxin derivatives can act as tubulin

polymerization inhibitors interacting with the colchicine-binding site. The synthesis and biological studies helped to develop a class of antitubulin agents for probing lead compounds and also a direction for further structure modification to obtain more potent anti-tumor drugs.

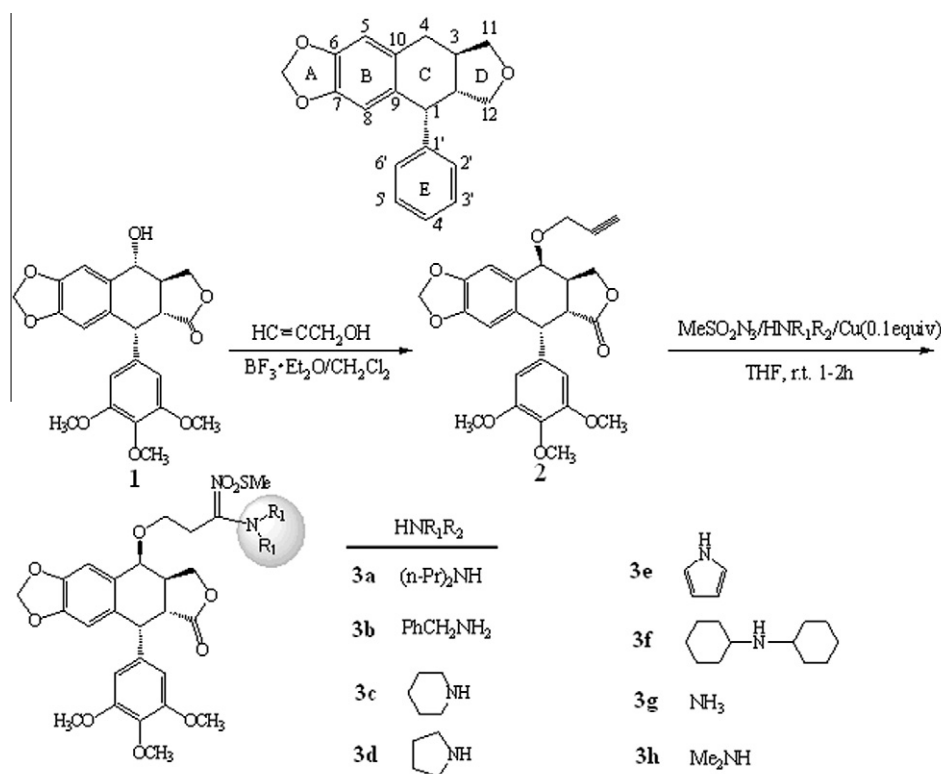
## 2. Results and discussion

### 2.1. Chemistry

As shown in Scheme 1, starting from podophyllotoxin **1**, propargyl group was firstly introduced in the 4-position of **1** upon reaction with propargyl alcohol in the presence of  $\text{BF}_3 \cdot \text{Et}_2\text{O}$  to give intermediate 4 $\beta$ -O-propargylpodophyllotoxin **2** in 87% yield. Subsequently, we applied a highly efficient copper-catalyzed three-component coupling reaction, in which **2** react with methanesulfonyl azide and a wide range of amines to afford twelve novel 4 $\beta$ -O-Sulfonyl amidine derivatives of 4-deoxypodophyllotoxin **3a–h** in

**Table 1**  
In vitro Activity of synthesized Compounds (**3a–3h**) and positive controls (Colchicine and Podophyllotoxin) against the K562, SGC, HeLa and HepG2 Cell Lines

	IC <sub>50</sub> ( $\mu\text{M}$ )			
	K562	SGC-7901	HeLa	HepG2
<b>3a</b>	2.96 $\pm$ 0.03	2.87 $\pm$ 0.03	2.63 $\pm$ 0.03	2.14 $\pm$ 0.04
<b>3b</b>	12.07 $\pm$ 0.04	19.16 $\pm$ 0.02	11.23 $\pm$ 0.02	17.88 $\pm$ 0.02
<b>3c</b>	9.01 $\pm$ 0.03	18.20 $\pm$ 0.03	10.37 $\pm$ 0.02	57.14 $\pm$ 0.01
<b>3d</b>	8.34 $\pm$ 0.02	11.21 $\pm$ 0.04	5.99 $\pm$ 0.03	20.79 $\pm$ 0.02
<b>3e</b>	1.01 $\pm$ 0.02	1.36 $\pm$ 0.01	0.75 $\pm$ 0.03	0.79 $\pm$ 0.01
<b>3f</b>	2.61 $\pm$ 0.02	3.21 $\pm$ 0.02	4.33 $\pm$ 0.01	1.95 $\pm$ 0.02
<b>3g</b>	3.48 $\pm$ 0.03	4.31 $\pm$ 0.01	3.75 $\pm$ 0.02	2.87 $\pm$ 0.03
<b>3h</b>	5.18 $\pm$ 0.02	3.71 $\pm$ 0.03	2.58 $\pm$ 0.02	4.17 $\pm$ 0.02
Colchicine	0.55 $\pm$ 0.02	0.05 $\pm$ 0.02	0.10 $\pm$ 0.02	0.02 $\pm$ 0.03
Podophyllotoxin	4.51 $\pm$ 0.03	0.34 $\pm$ 0.02	0.14 $\pm$ 0.04	0.51 $\pm$ 0.02



**Scheme 1.**

suitable yields. The structures of compounds **3a–h** were well characterized by using  $^1\text{H}$  NMR,  $^{13}\text{C}$  NMR, IR and HR-MS.

## 2.2. Effects on in vitro proliferation of the tumor cell lines

The effect of the podophyllotoxin derivatives on the proliferation of tumor cancer cell lines was evaluated using four human tumor cell lines: human leukemia cell line K562, human gastric cancer cell line SGC-7901, human cervical carcinoma cell line HeLa and Human hepatocellular liver carcinoma cell line HepG2, which were treated with the range of 0 to 100  $\mu\text{M}$  of test compounds for

48 h. For screening potential anti-proliferation effects, colchicine and podophyllotoxin were treated as positive controls. As shown in Table 1, the  $IC_{50}$  values derived from in vitro screening studies of the synthesized compounds and the controls were summarized. The term of  $IC_{50}$  was defined as the compound concentration required to inhibit tumor cell proliferation by 50% and data are expressed as the Mean  $\pm$  SE from the dose-response curves of at least three independent experiments. As shown, compound **3e** possessed highest antiproliferative activities against all four cell lines with  $IC_{50}$  values of 1.01, 1.36, 0.75 and 0.79  $\mu\text{M}$ , while the compounds **3b**, **3c** and **3d** showed poor activities.

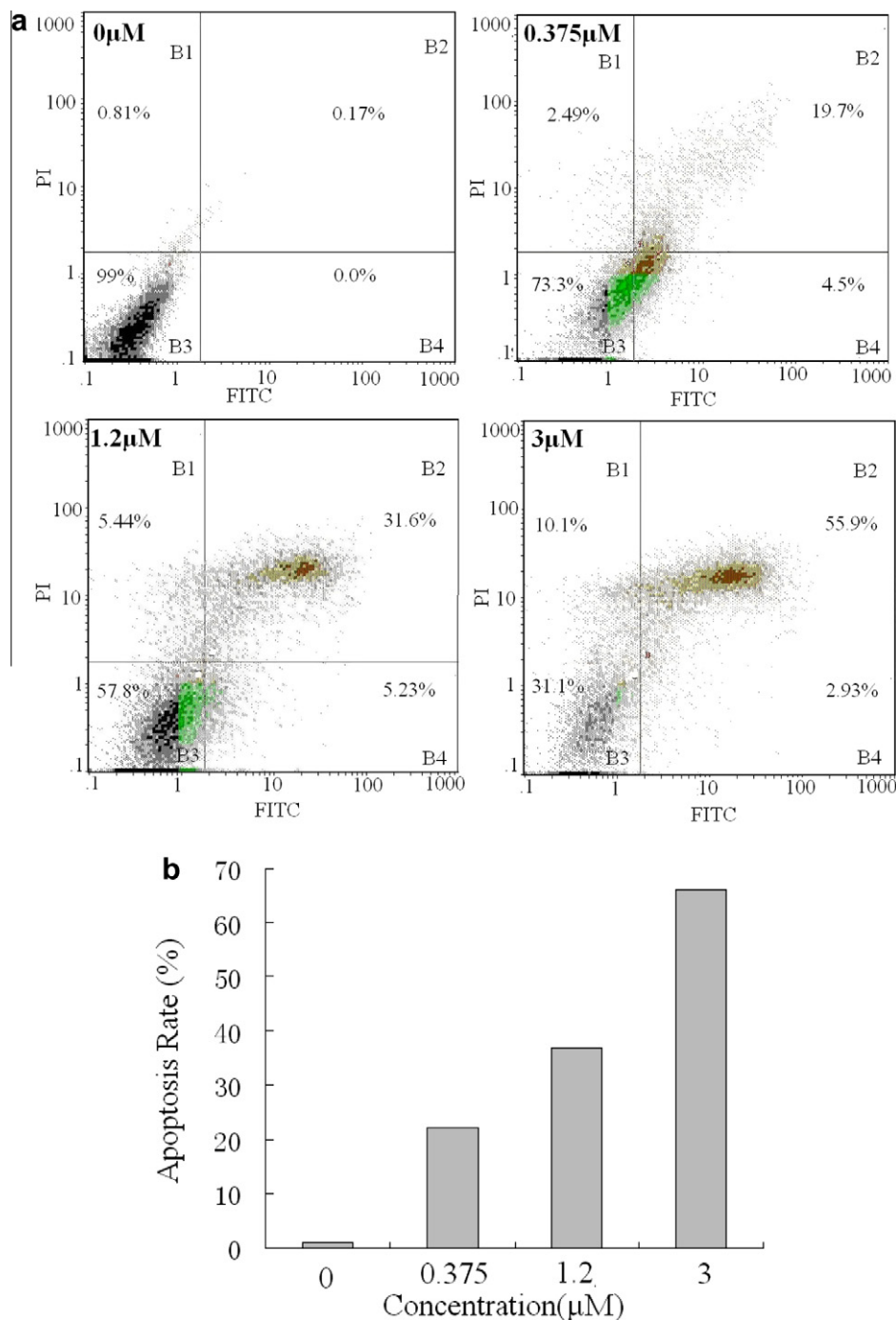


**Figure 1.** (a) Apoptosis effect on human leukemia K562 cell line induced by compound **3e**. The cells were incubated in media containing various concentration of **3e** (0, 0.375  $\mu\text{M}$ , 1.2  $\mu\text{M}$  and 3  $\mu\text{M}$ ) for 24 h. Cells and the amount of apoptotic cells was determined by flow cytometry using FITC-Annexin V/PI staining. (b) The rate of apoptotic cells as detected by flow cytometry. Cells in B1 and B2 quadrants were considered to be apoptotic cells. The experiment was repeated three times.

### 2.3. Effects on apoptosis

To probe whether compounds exhibiting high antiproliferative activity induced apoptosis of K562 cells, the cells were treated with the most potent antiproliferative compound **3e** to determine the percentage of cells. Flow cytometry was used to generate an apoptotic cell scatterplot of the control groups treated with compound **3e** (0, 0.375  $\mu$ M, 1.2  $\mu$ M and 3  $\mu$ M) for 24 h (Fig. 1a). The cell scatter could be composed of four subgroups as follows: B1 quadrant was the late apoptotic cells, B2 quadrant was the early apoptotic cells, B3 quadrant was the living cells, and B4 quadrant was the necrotic cells. For the different concentration of compound **3e**, the cells count in B1 and B2 quadrants were considered to be apoptotic cells and the total percentages were 0.98%, 22.19% and 37.04% and 66.0%, respectively (Fig. 1b). The results showed that the effect was observed in a dose-dependent manner and the apoptotic rates of K562 cells increased with the increase of concentration of **3e** (Fig. 1b). It demonstrated that the most active podophyllotoxin derivatives **3e** induced apoptosis of cells and thus as expected, caused the anticancer effects.

### 2.4. Analysis of cell cycle

From the in vitro tests it was found that **3e** significantly inhibited the growth of four human cancer cell lines. To determine whether the high anticancer effects of the compounds were caused by cell cycle accumulate at a certain phase, the cell cycle progression were therefore analyzed in K562 cells cultured for 36 h in the presence of increasing concentration of compound **3e** (0, 0.375  $\mu$ M, 1.2  $\mu$ M and 3  $\mu$ M) (Fig. 2a). As we known, the podophyllotoxin compounds were reported to exhibit strong activity on tubulin binding, which should induce the alteration of cell cycle parameters leading to a preferential G2/M blockade.<sup>27,28,35</sup> It can be seen from Fig. 2b, the cells accumulations in G2 phase of 10.87%, 50.91% and 82.49% were observed with 0.375  $\mu$ M, 1.2  $\mu$ M and 3  $\mu$ M treatment of **3e**, respectively, compared with 4.87% in untreated cultures. Moreover, the greatest accumulation of cells arrested in the G2/M stage occurred at 3  $\mu$ M, and a same concentration led to the greatest apoptosis. In parallel to the G2/M block (Fig. 2b), the cell cycle analysis showed a clear increase of proportion of sub-G1 cells, which always suggested the extensive DNA breakage. As shown, 1.17% of the cells were in sub-G1 phase for untreated cultures, whereas 2.26%, 7.43% and 13.73% of cells were in the sub-G1 phase with 0.375  $\mu$ M, 1.2  $\mu$ M and 3  $\mu$ M, respectively. In addition, a simultaneous sharp decrease in S and G1 cells occurred (Fig. 2b). All effect was observed in a dose-dependent manner. Thus, by two independent methods, it demonstrated that compound **3e** can obviously inhibit the proliferation of cancer cells K562 by arresting the cell cycle in a certain phase G2/M and inducing apoptosis.

### 2.5. Analysis of the inhibition effects of microtubule polymerization

To further explore whether the growth-inhibitory effect of the novel podophyllotoxin compounds was related to an interaction with the tubulin system, an inhibition assay on microtubule polymerization in vitro was performed. As shown in Figure 3a, the tubulin protein extracted from fresh goat brain tissue by two cycle polymerization-depolymerizations (as expressed in Experimental section) was purified to test the activity based on their polymerization and polymerization inhibition curve on different temperature (0 °C and 37 °C) by the fluorescent intensity. As indicated by the shape of curve, the purified protein showed perfect activities on polymerization for further assay. The inhibition effects of the most active compound **3e** with different concentrations (0, 10, 20, 40

and 60  $\mu$ M) on tubulin polymerization were monitored with colchicine and podophyllotoxin as reference compounds for comparison (Fig. 3b). The inhibition assay on the tubulin polymerization for the synthesized compounds was performed and **3e** showed the highest activity, which was consistent with the data in the cell proliferation assay. As expected, the compound **3e** on different concentrations caused a dose-dependent inhibition of tubulin polymerization in a similar way with positive control colchicine and podophyllotoxin as shown in Figure 3c. Compound **3e**, colchicine and podophyllotoxin showed 50% tubulin inhibition effects at 18.19, 23.35 and 24.03  $\mu$ M ( $IC_{50}$ ), respectively. The results strongly implicated a direct interaction between the compound **3e** and tubulin. It can be concluded that the antiproliferative activity of the compounds may derive from an interaction with tubulin and an interference with microtubule disassembly.

In addition, as we know, the classic tubulin binding agents, such as podophyllotoxin and their derivatives, were recognized to have damaging effects on vasculature. Thus, the effect of **3e** on the purified microtubule protein was also examined using transmission electron microscope. The structures of microtubules treated with DMSO (control) and **3e** were visualized. The normal interphase microtubules with DMSO solution exhibited typical reticular formation (Fig. 4a) on polymerization state at 37 °C, while the polymerization of microtubule was disturbed after treatment with **3e** at a concentration of 3  $\mu$ M. The complete inhibition effect of microtubules polymerization was illustrated in Figure 4b and the discrete club shaped cytoskeleton of tubulin was observed. The phenomena, combined with the cellular microtubule depolymerizing effects and the ability of **3e** to directly inhibit purified tubulin assembly, provided strong evidence that loss of function of microtubules in interphase cells treated with **3e** may prevent these cells from progressing into mitosis.

In summary, the relation of activities for the inhibition of microtubule polymerization and inhibition of proliferation provided an indication of tight linkage of antiproliferative effects and the compound's tubulin-dependent mechanisms of action. The antiproliferative activity of the compounds may derive from an interaction with tubulin and an interference with microtubule assembly. Compounds that effectively interfere with tubulin dynamics prevent mitosis in cancer cells, leading to cell cycle arrest and, eventually, apoptosis.

### 2.6. Analysis of molecular docking

As shown above, it could be hypothesized that the activity of podophyllotoxin-derived compounds could be due to their potential effects on tubulin depolymerisation. In order to strengthen the hypothesis, compound **3e**, the most active compound, was used as the representative one to investigate the binding modes of synthesized podophyllotoxin derivatives. Docking modes between **3e** and colchicine binding sites has been constructed and refined using molecular dynamics (MD) approach to offer a molecular level explanation with the binding behavior and to obtain more precise ligand–receptor models in the state close to natural conditions.

The average structure of compound **3e**-tubulin complex within the last 1 ns of the molecular dynamics trajectories was employed as refined binding model. As shown in Figure 5a, compound **3e** was exactly located within the colchicine binding pocket, the position of which was between the interfaces of  $\alpha$ - and  $\beta$ -subunit described as blue circle. The trimethoxyphenyl ring (E ring) of **3e** was inserted in a bigger hydrophobic cavity formed by  $\beta$ :Cys241,  $\beta$ :Leu248,  $\beta$ :A01a250,  $\beta$ :Lys254,  $\beta$ :Asn258,  $\beta$ :Ala317,  $\beta$ :Lys352 and  $\beta$ :Thr353, the other was suited in a less hydrophobic cavity formed by  $\alpha$ :Val177,  $\alpha$ :Ser178,  $\alpha$ :Thr179,  $\alpha$ :Tyr224 (Fig. 5a and Fig. 5b). This result indicated that the hydrophobic property was

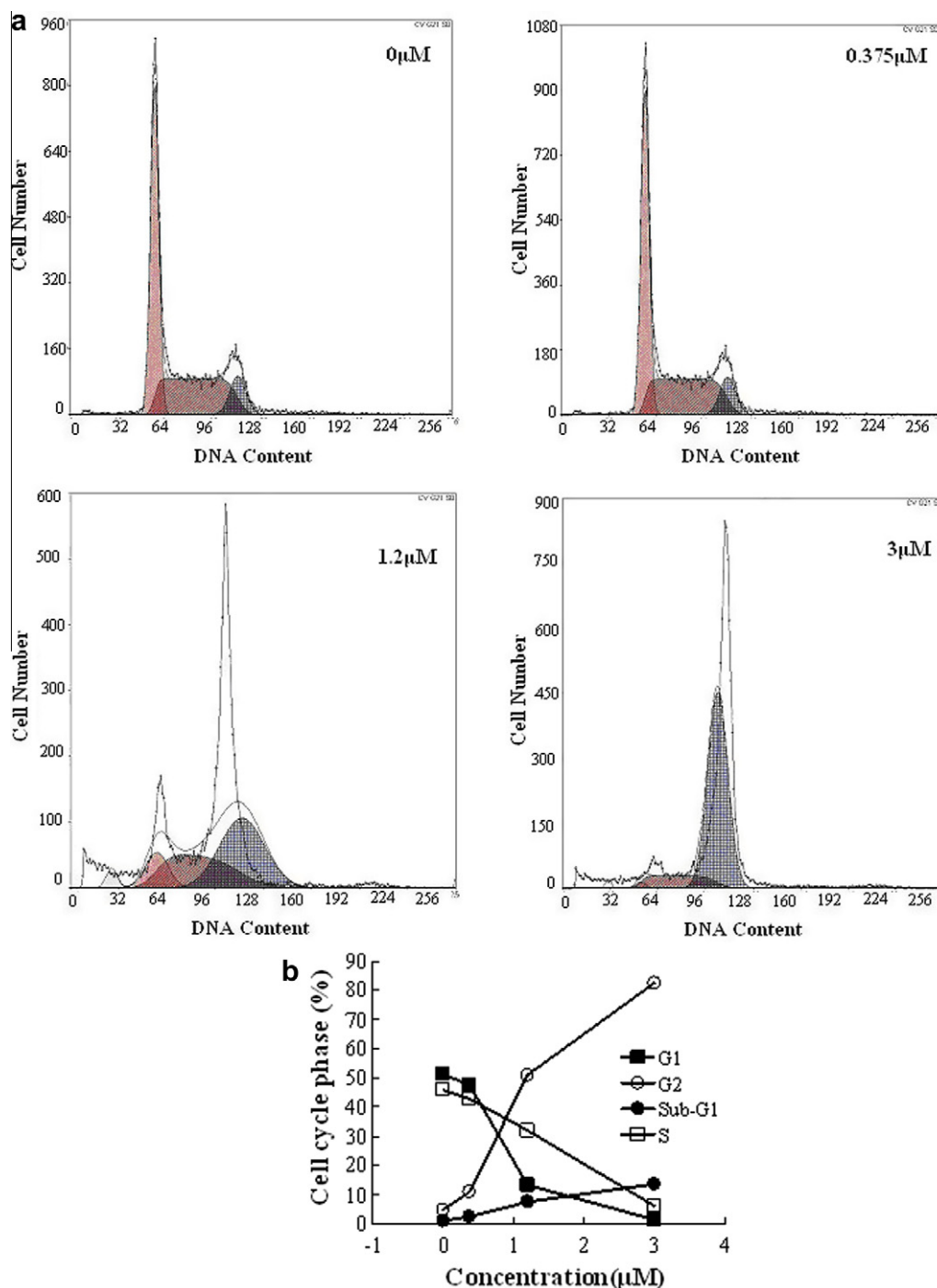


**Figure 2.** (a) Effects of compound **3e** on the cell cycle distribution of K562 cells. The cells were cultured for 36 h without the compound or with compound **3e** of 0.375 μM, 1.2 μM, and 3 μM inhibition of cell growth; (b) Quantitative analysis of cell cycle phase.

one of the main forces governing the interaction between **3e** and tubulin. On the other hand, the interaction was not exclusively hydrophobic. It should be noted that there were several ionic residues ( $\beta$ :Lys254, $\beta$ :Lys352), and polar residues ( $\alpha$ :Ser178, $\alpha$ :Thr179, $\alpha$ :Tyr224, $\beta$ :Asn258,  $\beta$ :Thr353) in the proximity to **3e**, which played important roles in stabilizing the tubulin-**3e** complex via electrostatic interaction and hydrogen bonds (Fig. 5a and Fig. 5c). The hydrogen-bonding or electrostatic interaction acted as an ‘anchor’, intensely determining the 3D space position of **3e** in the binding pocket and facilitating the hydrophobic interaction of the ligand **3e** with the side chain of protein. As shown in

Figure 5d, it can be found that the docking pocket was electro negative. In addition, amino residues  $\beta$ : Cys241 were just in the suitable position to form a hydrogen bond with O atom of **3e**. Hence, the amino acid residues with benzene ring can match that of **3e** in space to firm the conformation of the complex.

## 2.7. Analysis of binding free energy

In order to gain insight into the stability and dynamics properties of the complexes, further information about the forces involved in ligand binding can be obtained by analyzing the free

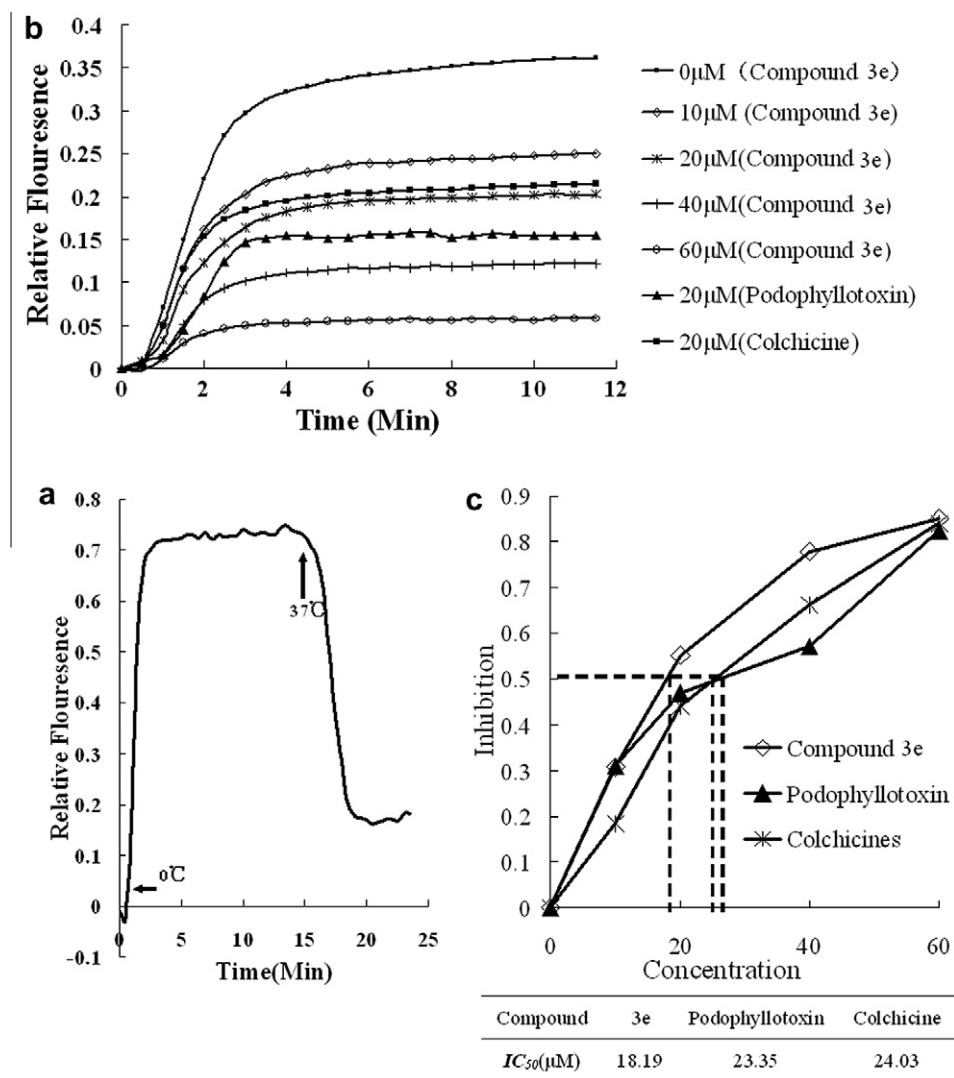


**Figure 3.** (a) Polymerization and inhibition of polymerization curve for tubulin pProtein; (b) Pattern of various concentrations of compound **3e** on in vitro tubulin polymerization assay; (c) Inhibition of tubulin polymerization by Compound **3e**, Podophyllotoxin (Control) and Colchicine (Control). All compounds were tested at different concentrations (0, 10, 20, 40 and 60  $\mu$ M).  $IC_{50}$  values were calculated based on the tubulin polymerization assay.

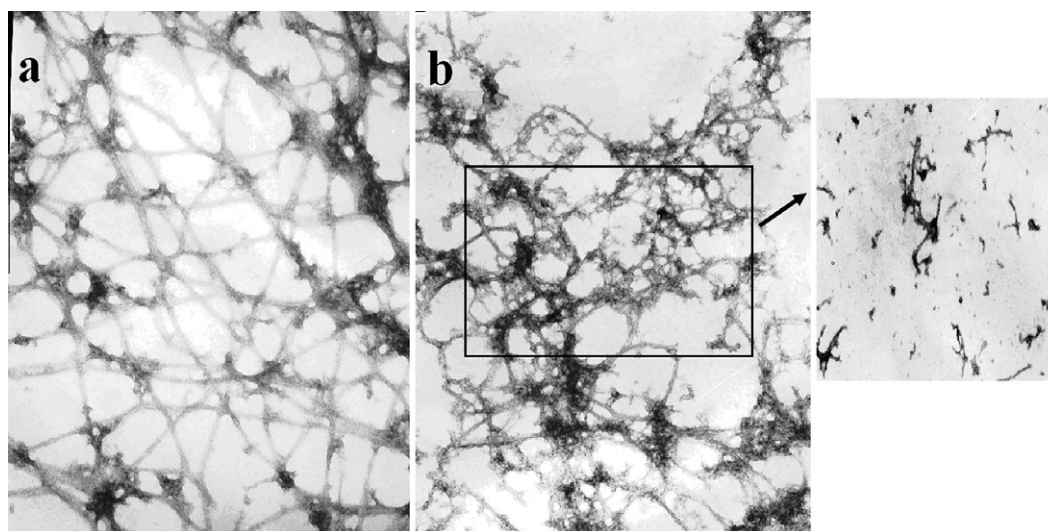


**Figure 4.** (a) Normal interphase microtubules; (b) Loss of interphase microtubules induced by compound **3e**.

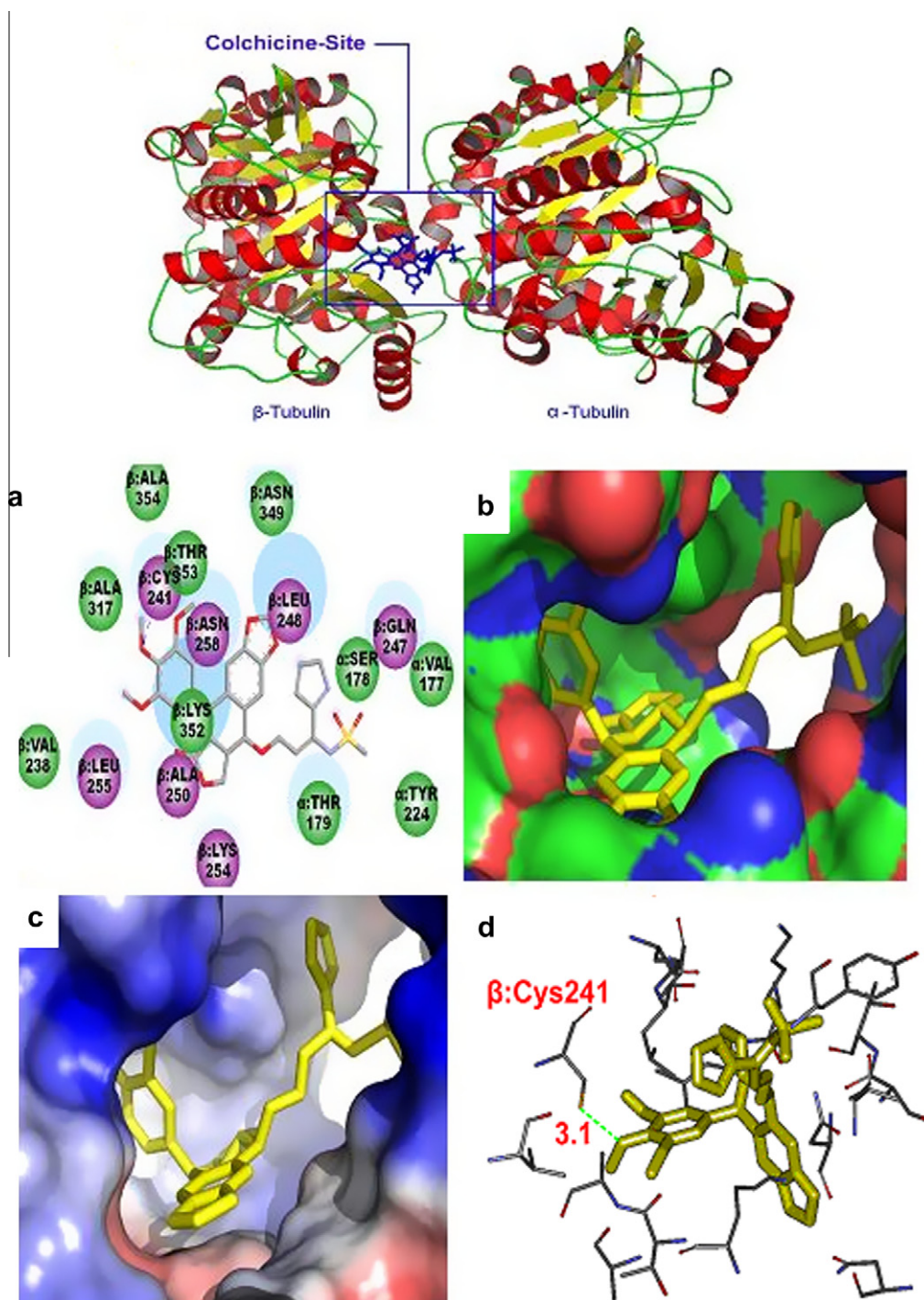


**Figure 5.** Binding mode between compound **3e** and tubulin. (a) 2D view; (b) Hydrophobic potentials plot on molecular surfaces (the colors of blue, green, white and red represent decreasing of hydrophobic potentials); (c) Electrostatic potentials plot on molecular surfaces (the colors of blue, white and red represent decreasing of electrostatic potentials); (d) 3D view.

energy contributions based on a more physically rigorous method MM-GBSA.

Firstly, some properties were examined by means of root-mean-square deviations (RMSD) values of different system with respect to the initial structure. As shown in Figure 6, the evolution of the RMSD values versus time for tubulin-**3e** complex using initial docking mode as a reference structure was obtained from the MD simulation. The calculated average RMSD fluctuation values of the complex was 2.5 Å after equilibrium indicating that the tubulin-**3e** complex structure was stable after 4 ns of simulation time.

In addition, the binding affinity of **3e** with tubulin was further calculated. The calculated free energy contributions for tubulin-**3e** complex were presented in Table 2. As shown, the term of  $\Delta E_{mm, ele}$  was negative, which generally means electrostatic interactions lead to favorable binding, whereas the term of  $\Delta G_{sol, pol}$  was positive, which means the electrostatic component of the solvation free energies is consistently unfavorable for binding. The data of non-polar component ( $\Delta E_{mm, vdw} + \Delta G_{sol, pol}$ ) was negative indicating that the contribution is favorable. In addition, from the quantitatively analysis of the non-polar ( $\Delta E_{mm, vdw} + \Delta G_{sol, npol}$ ) and the electrostatic ( $\Delta E_{mm, ele} + \Delta G_{sol, pol}$ ) contribu-

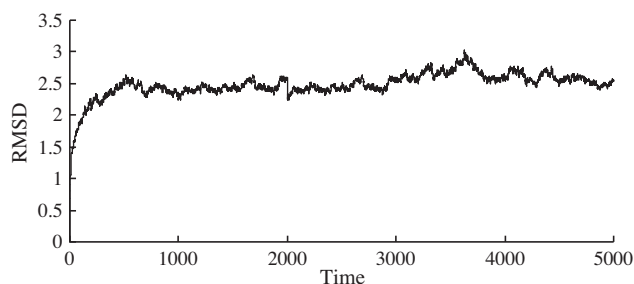


**Figure 6.** The RMSD values obtained during 5 ns of MD simulation for tubulin-**3e** complex.

tions for **3e**-tubulin complex, we came up with the conclusion that the interaction between **3e** and tubulin was dominated by more favorable nonpolar interactions, which was common for non-covalent association, rather than by electrostatic interactions.

Furthermore, to probe the importance of each residue, the energy contribution difference analysis was performed (Fig. 7). As shown, the most important residues were obtained with  $\alpha$ :Thr179,  $\alpha$ :Tyr224,  $\beta$ :Leu248,  $\beta$ :Leu255,  $\beta$ :Cys241, and  $\beta$ :Ala250, for which their contributions to the binding free energy were more than  $-10$  kcal/mol. Interestingly, these residues were found to form the core region of the colchicine binding site. Here, as expected, strongly favorable contributions to the binding were associated with the residues located in the active site. In addition, residues  $\alpha$ :Val177,  $\beta$ :Asn258,  $\beta$ :Ala317,  $\beta$ :Asn349,  $\beta$ :Lys352,  $\beta$ :Ala354 contributed weakly to the binding and  $\alpha$ :Thr179,  $\alpha$ :Tyr224,  $\beta$ :Leu248,  $\beta$ :Leu255,  $\beta$ :Cys241, and  $\beta$ :Ala250 made strong contributions (Fig. 7a). To represent the results more intuitively, the energy contributions of 6 key residues ( $\alpha$ :Thr179,  $\alpha$ :Tyr224,  $\beta$ :Leu248,  $\beta$ :Leu255,  $\beta$ :Cys241, and  $\beta$ :Ala250) were plotted in the active site for the **3e**-tubulin systems (Fig. 7b). It can be found that the non-polar residues ( $\beta$ : Leu248,  $\beta$ : Leu255,  $\beta$ : Ala250) contributed more to the binding free energy than the polar residues ( $\alpha$ : Thr179,  $\alpha$ : Tyr224,  $\beta$ : Cys241). Moreover, for all of the 6 key residues, hydrophobic interactions (black bar in the Figure) did favor for the binding behavior, while for residues  $\alpha$ : Thr179 and  $\beta$ : Leu248, the electrostatic interactions (red bar in the Figure) did disfavor for binding. From these results, we can conclude that hydrophobic interactions played the most important role in the binding affinity with **3e**. Thus, we believed that the hydrophobic interaction was the driven forces for the interaction between compound **3e** and tubulin protein although there were hydrogen bonds and electrostatic interactions.

### 3. Conclusion

In the present work, we synthesized a series of podophyllotoxin derivatives. The growth inhibition activities against various human cancer cell lines K562, SGC-7901, HeLa and HepG2 were tested and their biological mechanisms of activity of these synthetic compounds were investigated. Through the cell cycle and apoptosis analysis, compound **3e** which also showed the best proliferation activities exhibited strong ability to inhibit the proliferation of cancer cells K562 by arresting a massive accumulation in a certain phase G2/M and inducing a high levels of apoptosis. The direct

**Table 2**

The binding free energy components for tubulin-**3e** complex

Component	$\Delta E_{mm, ele}$	$\Delta E_{mm, vdW}$	$\Delta G_{sol, pol}$	$\Delta G_{sol, npol}$	$\Delta G_{ele, tol}$	$\Delta G_{np, tol}$	$\Delta G_{bind}$
Energy (kcal/mol)	-23.20	-83.56	68.77	-9.59	45.57	-93.15	-47.58

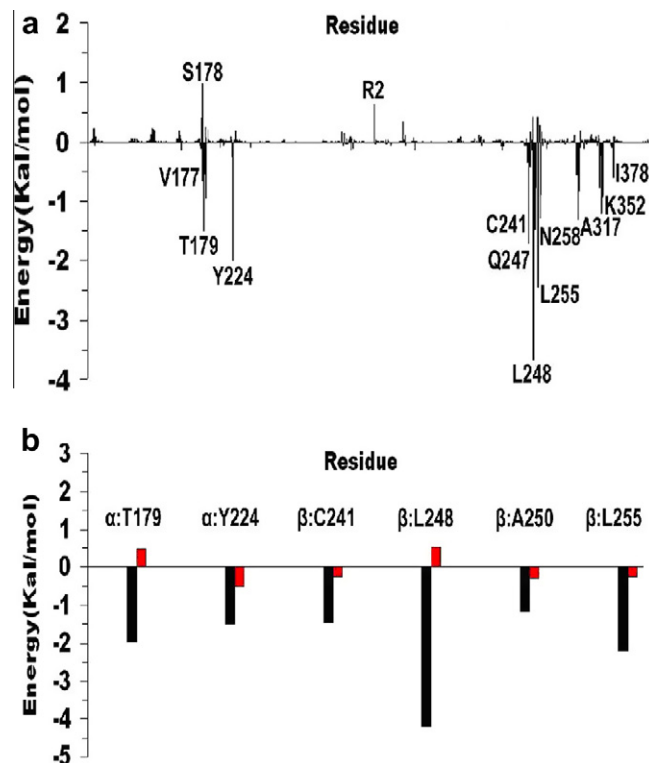


**Figure 7.** (a) Energy difference of each residue contribution to the binding of compounds **3e**; (b) Comparison of interactions between compound **3e** for key residues in the active site: black bar: Van der Waals and nonpolar solvation energy ( $\Delta E_{mm, vdW}$ ,  $\Delta G_{sol, npol}$ ) and red bar: electrostatic and polar solvation energy ( $\Delta E_{mm, ele}$ ,  $\Delta G_{sol, pol}$ ). The negative values are favorable and positive values are unfavorable for binding.

inhibition assay on the inhibition of polymerization for all of the series compounds demonstrated that **3e** exhibited the strong inhibition levels of polymerization for tubulin assemblage. All above results indicated that the synthesized compounds which effectively interfered with tubulin dynamics can prevent mitosis in cancer cells, thus leading to cell cycle arrest and, eventually a dose dependent apoptosis. In addition, the analysis of docking and molecular dynamic was consistent with the observed biological analysis for **3e**. The binding behavior of **3e** to tubulin was mainly stabilized by hydrophobic interaction, together with hydrogen-bonding interactions with Cys241 residue of  $\beta$ -tubulin. The synthesis and biological studies provided a class of lead compounds worthy of further investigation to obtain more potent anti-cancer drugs.

### 4. Experiments

#### 4.1. Chemistry

Melting points were taken on a Kofler melting point apparatus and are uncorrected; IR spectra were obtained on NIC-5DX spectrophotometer; mass spectral analysis was performed on a ZAB-HS and BrukerDaltonics APEXII49e instrument.  $^1\text{H}$  NMR and  $^{13}\text{C}$  NMR spectra were recorded at 400 MHz and 100 MHz on a Bruker

AM-400 spectrometer using TMS as reference (Bruker Company, USA). Podophyllotoxin $\mathbf{1}$  was isolated from a Chinese medicinal herb *Juniperus Sabina Linnaeus* and served as the starting material for the preparations of all the derivatives (shown in Scheme 1).

#### 4.1.1. Experimental procedure for the synthesis of podophyllotoxin derivatives 3a–3h (Scheme 1) 4-(prop-2-ynoxy) podophyllotoxin

$\text{BF}_3 \cdot \text{Et}_2\text{O}$  (0.36 ml) was added to a mixture of podophyllotoxin (1) (500 mg, 1.21 mmol) and Propargyl alcohol (135 mg, 2.4 mmol) in  $\text{CH}_2\text{Cl}_2$  (10 ml) at  $-20$ – $0$  °C with stirring. After 2 h, the reaction was quenched with pyridine (0.35 ml) and the mixture was extracted with EtOAc (100 ml). The extract was washed consecutively with cold dilute HCl and brine, dried over  $\text{MgSO}_4$ , and concentrated in vacuo. The residue was purified by silica gel column chromatography with EtOAc–Petroleum ether (1:4), gave  $\mathbf{2}$  (470 mg 90.9%).

#### 4.1.2. General synthetic procedure for compounds 3a–3h

To a stirred mixture of azide (0.6 mmol), 4 $\beta$ -O-propargylpodophyllotoxin $\mathbf{2}$  (0.5 mmol), and CuI (0.05 mmol) in  $\text{CH}_2\text{Cl}_2$  (10 mL) was slowly added the various amine nucleophile (0.6 mmol) at room temperature under an  $\text{N}_2$  atmosphere. Triethylamine (0.6 mmol) was added prior to the addition of nucleophiles. After the reaction was completed, which was monitored with TLC, the reaction mixture was diluted by adding  $\text{CH}_2\text{Cl}_2$  (5 mL) and aqueous  $\text{NH}_4\text{Cl}$  solution (6 mL). The mixture was stirred for an additional 30 min and two layers were separated. The aqueous layer was extracted with  $\text{CH}_2\text{Cl}_2$  (6 mL  $\times$  3). The combined organic layers were dried over  $\text{MgSO}_4$ , filtered, and concentrated in vacuo. The crude residue was purified by flash column chromatograph with an appropriate eluting solvent system.<sup>36</sup>

**4.1.2.1. Compound 3a.** 69% yield, white solid, mp 99–101 °C; IR  $\text{cm}^{-1}$ : 3425, 2928, 1776, 1589, 1551, 1483, 1269, 1125, 1039, 967, 776, 591;  $^1\text{H}$  NMR (400 MHz,  $\text{CDCl}_3$ )  $\delta$ : 6.92 (s, 1H, H-5), 6.51 (s, 1H, H-8), 6.24 (s, 2H, H-2', 6'), 5.96 (d,  $J$  = 10.0 Hz, 2H,  $\text{OCH}_2\text{O}$ ), 4.60 (d,  $J$  = 4.8 Hz, 1H, H-4), 4.38 (m, 1H, 11a-H), 4.26–4.09 (m, 2H, 11b, 1-H), 3.81 (s, 3H, 4'- $\text{OCH}_3$ ), 3.73 (s, 6H, 3', 5'- $\text{OCH}_3$ ), 3.38 (m, 2H, 1''-H), 3.31–3.16 (m, 2H, 2, 3-H), 3.09 (s, 3H,  $\text{Ms-CH}_3$ ), 1.64–1.50 (m, 6H, 2''-H and  $\text{N}(\text{CH}_2\text{CH}_3)_2$ ), 0.90–0.78 (m, 6H,  $\text{N}(\text{CH}_2\text{CH}_3)_2$ );  $^{13}\text{C}$  NMR (100 MHz,  $\text{CDCl}_3$ )  $\delta$ : 174.9, 164.6, 152.6 (2C, C-3', 5'), 148.4, 146.9, 137.2, 135.2, 132.0, 129.6, 109.7, 108.2 (2C, C-2', 6'), 101.5, 75.2, 68.2, 67.6, 60.7, 56.2 (2C, C-3', 5'- $\text{OCH}_3$ ), 51.4 (2C,  $\text{R}_1$ -1',  $\text{R}_2$ -1a'), 45.3, 43.9, 43.7, 41.1, 38.2, 31.7, 22.2 (2C,  $\text{R}_1$ -2',  $\text{R}_2$ -2a'), 11.1 (2C,  $\text{R}_1$ -3',  $\text{R}_2$ -3a'); HRMS  $m/z$  calcd for  $\text{C}_{32}\text{H}_{42}\text{N}_2\text{O}_{10}\text{S}$ : 647.2633  $[\text{M}+\text{H}]^+$ , found: 647.2639  $[\text{M}+\text{H}]^+$ .

**4.1.2.2. Compound 3b.** 67% yield, white solid, mp 107–109 °C; IR  $\text{cm}^{-1}$ : 3478, 2934, 1776, 1588, 1482, 1265, 1126, 1038, 935, 785, 582;  $^1\text{H}$  NMR (400 MHz,  $\text{CDCl}_3$ )  $\delta$ : 7.34–7.12 (m, 5H, Ph), 6.79 (s, 1H, H-5), 6.46 (s, 1H, H-8), 6.17 (s, 2H, H-2', 6'), 5.96 (d,  $J$  = 9.6 Hz, 2H,  $\text{OCH}_2\text{O}$ ), 4.47 (d,  $J$  = 4.8 Hz, 1H, H-1), 4.38 (m, 1H, 11a-H), 4.12–4.06 (m, 2H, 11b, 4-H), 3.94 (s, 2H,  $\text{PhCH}_2$ ), 3.80 (s, 3H, 4'- $\text{OCH}_3$ ), 3.73 (s, 6H, 3', 5'- $\text{OCH}_3$ ), 3.18 (m, 2H, 1''-H), 3.16–3.01 (m, 5H, 2, 3-H,  $\text{Ms-CH}_3$ ), 1.67 (m, 2H, 2''-H);  $^{13}\text{C}$  NMR (100 MHz,  $\text{CDCl}_3$ )  $\delta$ : 174.3, 165.5, 152.6 (2C, C-3', 5'), 148.5, 146.9, 137.2, 136.1, 135.1, 134.9, 131.9, 129.8, 129.0, 128.2, 127.9, 110.5, 109.6, 108.1 (2C, C-2', 6'), 101.5, 75.4, 67.2, 66.6, 60.7, 56.2 (2C, C-3', 5'- $\text{OCH}_3$ ), 46.1, 45.3, 43.8, 43.7, 41.0, 37.4, 34.4; HRMS  $m/z$  calcd for  $\text{C}_{33}\text{H}_{36}\text{N}_2\text{O}_{10}\text{S}$ : 653.2163  $[\text{M}+\text{H}]^+$ , found: 653.2147  $[\text{M}+\text{H}]^+$ .

**4.1.2.3. Compound 3c.** 56% yield, white solid, mp 114–116 °C; IR  $\text{cm}^{-1}$ : 3478, 2934, 1776, 1548, 1504, 1483, 1265, 1125, 1036, 931, 765, 531;  $^1\text{H}$  NMR (400 MHz,  $\text{CDCl}_3$ )  $\delta$ : 6.95 (s, 1H, H-5), 6.51 (s, 1H,

H-8), 6.24 (s, 2H, H-2', 6'), 5.98 (d,  $J$  = 9.6 Hz, 2H,  $\text{OCH}_2\text{O}$ ), 4.61 (d,  $J$  = 4.8 Hz, 1H, H-4), 4.54 (m, 1H, 11a-H), 4.37–4.22 (m, 2H, 11b, 1-H), 3.79 (s, 3H, 4'- $\text{OCH}_3$ ), 3.72 (s, 6H, 3', 5'- $\text{OCH}_3$ ), 3.57 (m, 2H, 1''-H), 3.25–3.20 (m, 2H, 2, 3-H), 3.02 (s, 3H,  $\text{Ms-CH}_3$ ), 2.83–2.16 (m, 4H, piperidine- $\text{CH}_2$ ), 1.74–1.25 (m, 6H, 2''-Hand piperidine);  $^{13}\text{C}$  NMR (100 MHz,  $\text{CDCl}_3$ )  $\delta$ : 174.8, 163.7, 152.6 (2C, C-3', 5'), 148.4, 146.9, 137.2, 135.1, 131.7, 129.5, 109.6, 108.3, 106.9 (2C, C-2', 6'), 101.5, 75.2, 67.8, 66.1, 60.7, 56.2 (2C, C-3', 5'- $\text{OCH}_3$ ), 48.2 (2C,  $\text{R}_1$ -1', 5'), 45.4, 43.9, 43.7, 38.2, 26.6, 25.3 (2C,  $\text{R}_1$ -2', 4'), 24.0; HRMS  $m/z$  calcd for  $\text{C}_{31}\text{H}_{38}\text{N}_2\text{O}_{10}\text{S}$ : 631.2320  $[\text{M}+\text{H}]^+$ , found: 631.2327  $[\text{M}+\text{H}]^+$ .

**4.1.2.4. Compound 3d.** 69% yield, white solid, mp 93–105 °C; IR  $\text{cm}^{-1}$ : 3425, 2928, 1776, 1589, 1551, 1483, 1269, 1125, 1039, 967, 776, 591;  $^1\text{H}$  NMR (400 MHz,  $\text{CDCl}_3$ )  $\delta$ : 6.88 (s, 1H, H-5), 6.52 (s, 1H, H-8), 6.23 (s, 2H, H-2', 6'), 5.97 (d,  $J$  = 10.0 Hz, 2H,  $\text{OCH}_2\text{O}$ ), 4.60 (d,  $J$  = 4.8 Hz, 1H, H-4), 4.38 (m, 1H, 11a-H), 4.26–4.09 (m, 2H, 11b, 1-H), 3.81 (s, 3H, 4'- $\text{OCH}_3$ ), 3.73 (s, 6H, 3', 5'- $\text{OCH}_3$ ), 3.38 (m, 2H, 1''-H), 3.31–16 (m, 2H, 2, 3-H), 3.03 (s, 3H,  $\text{Ms-CH}_3$ ), 2.82–2.16 (m, 4H, pyrrolidine- $\text{CH}_2$ ), 1.89–1.23 (m, 6H, 2''-H and pyrrolidine- $\text{CH}_2$ );  $^{13}\text{C}$  NMR (100 MHz,  $\text{CDCl}_3$ )  $\delta$ : 174.9, 163.7, 152.6 (2C, C-3', 5'), 148.4, 146.9, 137.2, 135.0, 131.9, 129.6, 110.5, 109.6, 108.1 (2C, C-2', 6'), 101.4, 75.2, 68.4, 67.5, 60.7, 56.2 (2C, C-3', 5'- $\text{OCH}_3$ ), 48.7 (2C,  $\text{R}_1$ -1', 4'), 48.6, 45.3, 43.6, 41.1, 38.2, 26.7, 25.7 (2C,  $\text{R}_1$ -2', 3'); HRMS  $m/z$  calcd for  $\text{C}_{30}\text{H}_{36}\text{N}_2\text{O}_{10}\text{S}$ : 617.2163,  $[\text{M}+\text{H}]^+$ , found: 617.2156  $[\text{M}+\text{H}]^+$ .

**4.1.2.5. Compound 3e.** 26% yield, white solid, mp 132–134 °C; IR  $\text{cm}^{-1}$ : 3415, 2924, 1774, 1557, 1505, 1481, 1265, 1124, 1041, 926, 761, 516;  $^1\text{H}$  NMR (400 MHz,  $\text{CDCl}_3$ )  $\delta$ : 7.10 (s, 1H, pyrrole-H), 7.00 (s, 1H, H-5), 6.52 (s, 1H, H-8), 6.34 (s, 2H, pyrrole-H), 6.21 (s, 2H, H-2', 6'), 5.96 (d,  $J$  = 9.6 Hz, 2H,  $\text{OCH}_2\text{O}$ ), 4.64 (d,  $J$  = 5.2 Hz, 1H, H-4), 4.54 (m, 1H, 11a-H), 4.22–4.12 (m, 2H, 11b, 1-H), 3.80 (s, 3H, 4'- $\text{OCH}_3$ ), 3.72 (s, 6H, 3', 5'- $\text{OCH}_3$ ), 3.48 (m, 2H, 1''-H), 3.27–3.10 (m, 5H, 2, 3-H,  $\text{Ms-CH}_3$ ), 1.68 (m, 2H, 2''-H);  $^{13}\text{C}$  NMR (100 MHz,  $\text{CDCl}_3$ )  $\delta$ : 174.9, 152.6 (2C, C-3', 5'), 148.4, 147.5, 137.2, 135.4, 132.3, 130.6, 129.1, 127.0, 112.3, 110.8, 109.5, 108.2 (2C, C-2', 6'), 107.0, 101.4, 74.7, 68.0, 67.3, 60.7, 56.2 (2C, C-3', 5'- $\text{OCH}_3$ ), 45.4, 44.0, 43.1, 40.8, 38.3, 29.7; HRMS  $m/z$  calcd for  $\text{C}_{30}\text{H}_{32}\text{N}_2\text{O}_{10}\text{S}$ : 612.178  $[\text{M}+\text{H}]^+$ , found: 612.182  $[\text{M}+\text{H}]^+$ .

**4.1.2.6. Compound 3f.** 50% yield, white solid, mp 122–124 °C; IR  $\text{cm}^{-1}$ : 3448, 2931, 1778, 1541, 1504, 1481, 1269, 1127, 1038, 932, 767, 515;  $^1\text{H}$  NMR (400 MHz,  $\text{CDCl}_3$ )  $\delta$ : 6.99 (s, 1H, H-5), 6.50 (s, 1H, H-8), 6.36 (s, 2H, H-2', 6'), 5.96 (s, 2H,  $\text{OCH}_2\text{O}$ ), 4.64–4.63 (m, 2H, 4-H, 1-H), 4.57 (m, 1H, 11a), 4.00 (m, 1H, 11b), 3.81 (s, 3H, 4'- $\text{OCH}_3$ ), 3.75 (s, 6H, 3', 5'- $\text{OCH}_3$ ), 3.37 (m, 2H, 1''-H), 3.28–3.19 (m, 2H, 2, 3-H), 3.00 (s, 3H,  $\text{Ms-CH}_3$ ), 2.89–2.80 (m, 2H, cyclohexyl-CH), 1.78–1.24 (m, 22H, 2''-H and cyclohexyl- $\text{CH}_2$ );  $^{13}\text{C}$  NMR (100 MHz,  $\text{CDCl}_3$ )  $\delta$ : 174.9, 163.0, 152.1 (2C, C-3', 5'), 148.4, 147.1, 137.3, 135.4, 131.7, 130.5, 109.8, 108.5 (2C, C-2', 6'), 106.8, 101.4, 75.2, 71.3, 65.6 (2C,  $\text{R}_1$ -1',  $\text{R}_2$ -1a'), 60.7, 59.7, 56.4 (2C, C-3', 5'- $\text{OCH}_3$ ), 45.4, 43.9, 43.6, 37.8, 30.9 (4C,  $\text{R}_1$ -2', 6',  $\text{R}_2$ -2a', 6a'), 29.4 (2C,  $\text{R}_1$ -4',  $\text{R}_2$ -4a'), 25.0 (4C,  $\text{R}_1$ -3', 5',  $\text{R}_2$ -3a', 5a'); HRMS  $m/z$  calcd for  $\text{C}_{38}\text{H}_{50}\text{N}_2\text{O}_{10}\text{S}$ : 727.3259  $[\text{M}+\text{H}]^+$ , found: 727.3239  $[\text{M}+\text{H}]^+$ .

**4.1.2.7. Compound 3g.** 72% yield, white solid, mp 116–118 °C; IR  $\text{cm}^{-1}$ : 3421, 2927, 1776, 1566, 1503, 1483, 1267, 1124, 1038, 932, 770, 574;  $^1\text{H}$  NMR (400 MHz,  $\text{CDCl}_3$ )  $\delta$ : 6.89 (s, 1H, H-5), 6.53 (s, 1H, H-8), 6.24 (s, 2H, H-2', 6'), 5.97 (d,  $J$  = 8.8 Hz, 2H,  $\text{OCH}_2\text{O}$ ), 4.60 (d,  $J$  = 5.2 Hz, 1H, H-4), 4.38 (m, 1H, 11a-H), 4.24–4.12 (m, 2H, 11b, 1-H), 3.81 (s, 3H, 4'- $\text{OCH}_3$ ), 3.74 (s, 6H, 3', 5'- $\text{OCH}_3$ ), 3.33 (m, 2H, 1''-H), 3.28–3.10 (m, 2H, 2, 3-H), 3.09 (s, 6H,  $\text{N}(\text{CH}_3)_2$ ), 3.04 (s, 3H,  $\text{Ms-CH}_3$ ), 1.64 (m, 2H, 2''-H);  $^{13}\text{C}$  NMR (100 MHz,  $\text{CDCl}_3$ )  $\delta$ : 174.8, 165.7, 152.6 (2C, C-3', 5'), 148.4, 146.9, 137.2,

135.1, 132.0, 129.3, 109.6, 108.2 (2C, C-2', 6'), 106.8, 101.4, 75.2, 67.9, 67.4, 60.7, 56.2 (2C, C-3', 5'-OCH<sub>3</sub>), 45.4, 43.9, 43.6, 41.1, 39.3 (2C, R<sub>1</sub>-1', R<sub>2</sub>-1a'), 38.2; HRMS *m/z* calcd for C<sub>28</sub>H<sub>34</sub>N<sub>2</sub>O<sub>10</sub>S:591.2007 [M+H]<sup>+</sup>, found: 591.2017 [M+H]<sup>+</sup>.

**4.1.2.8. Compound 3h.** 74% yield, white solid, mp 111–113 °C; IR cm<sup>-1</sup>: 3418, 3333, 2928, 1774, 1585, 1505, 1482, 1273, 1124, 1037, 932, 787, 586; <sup>1</sup>H NMR (400 MHz, CDCl<sub>3</sub>) δ: 6.82 (s, 1H, H-5), 6.55 (s, 1H, H-8), 6.32 (s, 2H, H-2',6'), 5.99 (s, 2H, OCH<sub>2</sub>O), 4.60–4.51 (m, 2H, H-4 and 11a-H), 4.23–4.15 (m, 2H, 11b,1-H), 3.80 (s, 3H, 4'-OCH<sub>3</sub>), 3.74 (s, 6H, 3',5'-OCH<sub>3</sub>), 3.34 (m, 2H, 1''-H), 2.98–2.95 (m, 5H, 2,3-H, Ms-CH<sub>3</sub>), 1.58 (m, 2H, 2''-H); <sup>13</sup>C NMR (100 MHz, CDCl<sub>3</sub>) δ: 174.6, 166.4, 152.6 (2C, C-3', 5'), 148.7, 146.9, 137.3, 135.2, 132.3, 128.5, 110.9, 109.2, 108.2, 101.6, 75.3, 67.2, 66.4, 60.7, 56.2 (2C, C-3', 5'-OCH<sub>3</sub>), 45.3, 43.9, 42.0, 41.1, 38.1; HRMS *m/z* calcd for C<sub>26</sub>H<sub>30</sub>N<sub>2</sub>O<sub>10</sub>S:563.1694 [M+H]<sup>+</sup>, found: 563.1679 [M+H]<sup>+</sup>.

## 4.2. Cell culture and inhibition of the cell growth

Four independent human tumor cell lines: human leukemia cell line K562, human gastric cancer cell line SGC-7901, human cervical carcinoma cell line HeLa and Human hepatocellular liver carcinoma cell line HepG2 were obtained from key lab of preclinical study for new drugs of Gausu province of Lanzhou university. All test compounds were dissolved in dimethyl sulfoxide (DMSO) at 1 mg/mL immediately before use and diluted in the medium before addition to the cells. All cell lines were cultured in an RPMI 1640 medium (GIBCO) supplemented with 10% bovine fetal calf serum, 2 mM L-glutamine (GIBCO), 10 mM β-mercaptoethanol, 100U/mL of penicillin, and 100 μg/mL of streptomycin. Cells (2 × 10<sup>5</sup> cells in 100 mL medium) in their log phase of growth were seeded in 96-well microtitre plates. After 24 h of incubation at 37 °C and 5% CO<sub>2</sub> to allow cell attachment, cultures were treated with varying concentrations (0–100 μM) of test compounds. For each concentration, five replicate wells were used. Considering the possible antiproliferative effects of DMSO, the concentration of DMSO in the array was less than 0.1% and will not affect the cell growth of the cell lines. The cell growth was calculated by subtracting mean OD value of the respective blank from the mean OD value of experimental set. Percentage of growth in the presence of test compounds was calculated considering the growth in the absence of any test compounds as 100% and the results are reported in terms of IC<sub>50</sub> (concentration causing 50% inhibition relative to untreated controls) values.

## 4.3. Cell cycle analysis and apoptosis detection

Flow cytometry was used to measure cell cycle profile and apoptosis. For cell cycle analysis, K-562 cells (1 × 10<sup>5</sup>) treated with compounds **3e** with various concentration (0 μM, 0.375 μM, 1.2 μM and 3 μM) were washed twice with ice-cold PBS, harvested, fixed with ice cold PBS in 70% ethanol and stored at –20 °C for 30 min. After fixation, these cells were incubated with RNase A (0.1 mg/mL) at 37 °C for 30 min, stained with propidium iodide (50 μg/mL) for 30 min on ice in dark. Cells were harvested by centrifugation and further stained with DNA staining solution (10 mg). The DNA contents were then detected by flow cytometer and the cell cycle profile was analyzed from the DNA content histograms.<sup>37</sup>

Flow cytometry with FITC-Annexin V/PI double staining Trypsin (Sigma) without EDTA was used to digest and collect the control group and the cells treated with 0.375 μM, 1.2 μM, and 3 μM compound **3e**. Flow cytometry was performed according to the apoptosis detection kit procedures. The K562 cells were washed with PBS twice, centrifuged at 300×g for 5 min, and 5 × 10<sup>5</sup> cells were collected. Binding buffer suspension (500 μl) was added to

the cells, and then 5 μl of the FITC-Annexin V mix was added. Next, 5 μl of the PI mix was added, and the suspension was mixed and kept at room temperature in the dark for 15 min of reaction. Flow cytometry was performed using a FACSCalibur Xow cytometer (BD Biosciences, CA, USA).

## 4.4. Separation of active microtubule protein

The goat brains (1.8 kg) were homogenized in a Waring blender and then centrifuged in the cold at 32 800 rpm for 1 h. The supernatant was accumulated and divided into four aliquots. ATP and GTP were added to aliquot at 37 °C, incubated and centrifuged. The supernatants were discarded, and the pellets were homogenized. After 30 min on ice, the very viscous suspension was centrifuged in the cold for 30 min. The pellet was re-homogenized sequentially 2 times and the cold centrifugation was repeated each time. All supernatants were pooled and the cold pellets were set aside. To each 100 mL of the combined supernatant were added 55.3 g of glycerol (4 M) and 5 mL of a solution containing Mes (pH 6.4), EGTA, MgCl<sub>2</sub>, 2-mercaptoethanol, and EDTA to maintain the concentrations of these components and ATP and GTP for final concentrations of 1 and 0.3 mM. The mixture was incubated at 37 °C for 1 h and centrifuged in the warm for 1 h at 32,000 rpm and the warm supernatant was set aside. The suspension was left on ice for 30 min and centrifuged in the cold for 30 min. Very small cold pellets are obtained and then were combined with the previous cold pellets. Preparation of the microtubule protein was outlined in reference.<sup>38</sup>

## 4.5. In vitro tubulin polymerization analysis

To evaluate the effect of the compounds on tubulin assembly in vitro the test compounds were incubated across a concentration range with 10 μM tubulin together with buffer containing 20% glycerol and 1 mM ATP at 37 °C and then cooled to 0 °C. The effect of the test compounds on tubulin polymerization was observed turbidimetrically using a fluorescent plate reader.<sup>39</sup> The IC<sub>50</sub> value was defined as the compound concentration that inhibited the extent of assembly by 50%.

To observe the effect of polymerization inhibition of the tubulin protein, electron micrographs were used. Tubulins were incubated with or without Compound **3e** in assay buffer (80 mM PIPES (pH 6.9), 1 mM MgCl<sub>2</sub>, and 1 mM EDTA) containing 30% glycerol and 1 mM GTP for 30 min at 37 °C. Samples were fixed by dilution (1:20 –1:50 fold) into assay buffer containing 30% glycerol and 0.5% glutaraldehyde at 37 °C, and then 10 ml of each sample were spotted onto Formavar-coated grids and stained with uranyl acetate for 30 s. Electron micrographs were obtained using a Philips CM12 transmission electron microscope with an accelerating voltage of 100 kV.

## 4.6. Molecular modeling

The docking mode was based on the podophyllotoxin-cinchicoline complex structure (PDB code: 1SA1). Water molecules, co-crystallized ligand and ions were removed and the missing hydrogens and Kollman partial charges were added. The structure of compound **3e** was built with Gview and optimized at the B3LYP/6–31++G\*\* level by Gaussian 98 software. Docking simulations were performed with AutoDock4.0<sup>40</sup> using a Lamarckian genetic algorithm. The large enough grid volumes were considered and determined by the need to maintain a small grid spacing (0.375) for the search box and at the same time to perform the docking calculation without neglecting any portion of the protein surface. The others docking parameters were set as default. During docking,

a maximum number of 100 conformers were considered, and the root-mean-square (RMS) cluster tolerance was set to 2.0 Å

#### 4.7. Molecular dynamics simulations

The MD simulation was carried out with AMBER software (version 11),<sup>41</sup> using AMBER ff02 force field for protein and the general AMBER force field (GAFF) as topology parameters for compound **3e**. The optimized geometries of **3e** were employed and hydrogen atoms were added to the initial **3e**-tubulin complex model using the tleap module, setting ionizable residues as their default protonation states at a neutral pH value. The complex were then solvated in a cubic periodic box of explicit TIP3P water model that extended a minimum 10 Å distance from the box surface to any atom of the solute. All bond lengths involving hydrogens were constrained using the SHAKE algorithm and integration time step was set to 2 fs using the Verlet leapfrog algorithm. After the heating phase, a 5 ns MD simulation was performed under 1 atm and constant temperature of 300 K with the NPT ensemble. Constant temperature was maintained using the Langevin thermostat with a collision frequency of  $2\text{ ps}^{-1}$  and constant pressure was maintained employing isotropic position scaling algorithm with a relaxation time of 2 ps. The values of the binding free energies ( $\Delta G_{\text{bind}}$ ) of complexes was calculated using the MM-GBSA approach implemented as script (MMPBSA.py) in AMBER software.<sup>42</sup> As ns many as 500 equidistant snapshots (every 2 ps) have been extracted from the last 1 ns stable MD trajectory of the complex and counterions and explicit water molecules were removed from the snapshots.

#### Acknowledgments

This work was financially supported by the Fundamental Research Funds for the Central Universities (Izujbky-2010-134); National Natural Science Foundation of China (NO. 31000017) (NO. 21102065) (NO. 21207056) and the Natural Foundation of Gansu Province (1104WCGA187).

#### References and notes

- Kim, D. Y.; Kim, K. H.; Kim, N. D.; Lee, K. Y.; Han, C. K.; Yoon, J. H.; Moon, S. K.; Lee, S. S.; Seong, B. L. *J. Med. Chem.* **2006**, *49*, 5664.
- Zhou, J.; Giannakakou, P. *Curr. Med. Chem. Anticancer Agents* **2005**, *5*, 65.
- Pichichero, M. E.; Avers, C. J. *Subcell. Biochem.* **1973**, *2*, 97.
- Wang, H. W.; Nogales, E. *Nature* **2005**, *433*, 911.
- Gourley, M.; Williamson, J. S. *Curr. Pharm. Des.* **2000**, *6*, 417.
- Romagnoli, R.; Baraldi, P. G.; Pavani, M. G.; Tabrizi, M. A.; Preti, D.; Fruttarolo, F.; Piccagli, L.; Jung, M. K.; Hamel, E.; Borgatti, M.; Gamba, R. *J. Med. Chem.* **2006**, *49*, 3906.
- Jordan, A.; Hadfield, J. A.; Lawrence, N. J.; McGown, A. T. *Med. Res. Rev.* **1998**, *18*, 259.
- Nogales, E.; Wolf, S. G.; Downing, K. H. *Nature* **1998**, *391*, 199.
- Liou, J. P.; Chang, C. W.; Song, J. W.; Yang, Y. N.; Yeh, C. F.; Tseng, H. Y.; Lo, Y. K.; Chang, Y. L.; Chang, C. M.; Hsieh, H. P. *J. Med. Chem.* **2002**, *45*, 2556.
- Hsieh, H. P.; Liou, J. P.; Lin, Y. T.; Mahindroo, N.; Chang, Y. L.; Yang, Y. N.; Chern, S. S.; Tan, U. K.; Chang, C. W.; Chen, T. W.; Lin, C. H.; Chang, Y. Y.; Wang, C. C. *Med. Chem. Lett.* **2003**, *13*, 101.
- Liou, J. P.; Chang, J. Y.; Chang, C. W.; Chang, C. Y.; Maindroo, N.; Kuo, F. M.; Hsieh, H. P. *J. Med. Chem.* **2004**, *47*, 2897.
- Thorpe, P. E.; Chaplin, D. J.; Blakey, D. C. *Cancer Res.* **2003**, *63*, 1144.
- Tozer, G. M.; Kanthou, C.; Parkins, C. S.; Hill, S. A. *Int. J. Exp. Pathol.* **2002**, *83*, 21.
- Pettit, G. R.; Singh, S. B.; Hamel, E.; Lin, C. M.; Alberts, D. S.; Garcia-Kendall, D. *Experientia* **1989**, *45*, 209–211.
- Lin, C. M.; Ho, H. H.; Pettit, G. R.; Hamel, E. *Biochemistry* **1989**, *28*, 6984.
- Chou, K. C.; Zhang, C. T.; Maggiora, G. M. *Biopolymers* **1994**, *34*, 143.
- Nettles, J. H.; Li, H.; Cornett, B.; Krahn, J. M.; Snyder, J. P.; Downing, K. H. *Science* **2004**, *305*, 866.
- Honess, D. J.; Stratford, M. R.; Wilson, J.; Tozer, G. M. *Int. J. Oncol.* **2003**, *21*, 717.
- Vitale, I.; Antoccia, A.; Cenciarelli, C.; Crateri, P.; Meschini, S.; Arancia, G.; Pisano, C.; Tanzarella, C. *Apoptosis* **2006**, *12*, 155.
- Cecchi, P. M.; Nettles, J. H.; Zhou, J.; Snyder, J. P.; Joshi, H. C. *Trends. Pharmacol. Sci.* **2003**, *4*, 2361.
- Li, Q.; Sham, H. L. *Expert. Opin. Ther. Pat.* **2002**, *12*, 1663.
- Jordan, M. A. *Curr. Med. Chem.* **2002**, *2*, 1.
- Nam, N. H. *Curr. Med. Chem.* **2003**, *10*, 1697.
- Pettit, G. R.; Toki, B.; Herald, A. L.; Verdier-Pinard, P.; Boyd, M. R.; Hamel, E.; Pettit, R. K. *J. Med. Chem.* **1998**, *41*, 1688.
- Cassady, J. M.; Dourous, J. D. *Anticancer agents based on natural product models. In The Anticancer Agents based on Natural Product Models*; Cassady, J., Dourous, M. J., Eds.; Academic Press: New York, 1980; p 319.
- Zhang, Y. J.; Litaudon, M.; Bousserouel, H.; Martin, M. T.; Thoison, O.; Léonce, S.; Dumontet, V.; Sévenet, T.; Guéritte, F. *J. Nat. Prod.* **2007**, *70*, 1368.
- Castro, M. A.; Miguel del Corral, J. M.; Gordaliza, M.; García, P. A.; Gómez-Zurita, M. A.; García-Grávalos, M. D.; de la Iglesia-Vicente, J.; Gajate, C.; An, F.; Mollinedo, F.; San Feliciano, A. *J. Med. Chem.* **2004**, *47*, 1214.
- Abad, A.; López Pérez, J. L.; Del Olmo, E.; García-Fernández, L. F.; Francesch, A. M.; Trigili, C.; Barasoain, I.; Andreu, J. M.; Díaz, J. F.; San Feliciano, A. *J. Med. Chem.* **2012**, *55*, 6724.
- Che, C.; Yang, G. Q.; Thiot, C.; Lacoste, M. C.; Currie, J. C.; Demeule, M.; Regina, A.; Beliveau, R.; Castaigne, J. P. *J. Med. Chem.* **2010**, *53*, 2814.
- Ettinger, D. S.; Finkelstein, D. M.; Ritch, P. S.; Lincoln, S. T.; Blum, R. H. *Lung Cancer* **2002**, *37*, 311.
- Abad, A.; López-Pérez, J. L.; Del Olmo, E.; García-Fernández, L. F.; Francesch, A.; Trigili, C.; Barasoain, I.; Andreu, J. M.; Díaz, J. F.; San Feliciano, A. *J. Med. Chem.* **2012**, *55*, 6724.
- Dumontet, C.; Jordan, M. A. *Nat. Rev. Drug Discov.* **2010**, *9*, 790.
- Mustafa, J.; Khan, S. I.; Ma, G.; Walker, L. A.; Khan, I. A. *Lipids* **2004**, *39*, 659.
- Mustafa, J.; Khan, S. I.; Ma, G.; Walker, L. A.; Khan, I. A. *Lipids* **2004**, *39*, 167.
- Gambari, R.; Terada, M.; Bank, A.; Rifkind, R. A.; Marks, P. A. *Proc. Natl. Acad. Sci. U.S.A.* **1978**, *75*, 3801.
- Liu, Y. Q.; Li, L. H.; Li, W. Q.; Feng, G.; Yang, L. *Chem. Pap.* **2011**, *65*, 739.
- Hamel, E.; Lin, C. M. *Biochemistry* **1984**, *23*, 4173.
- Duan, J. X.; Cai, X.; Meng, F.; Lan, L.; Hart, C.; Matteucci, M. *J. Med. Chem.* **2007**, *50*, 1001.
- Morris, G. M.; Goodsell, D. S.; Halliday, R. S.; Huey, R.; Hart, W. E.; Belew, R. K.; Olson, A. J. *J. Comput. Chem.* **1998**, *19*, 1639.
- Case, D. A.; Darden, T. A.; Cheatham, T. E.; Simmerling, C. L.; Wang, J.; Duke, R. E.; Luo, R.; Walker, R. C.; Zhang, W.; Merz, K. M.; Roberts, B.; Wang, B.; Hayik, S.; Roitberg, A.; Seabra, G.; Kolossvai, I.; Wong, K. F.; Paesani, F.; Vanicek, J.; Liu, J.; Wu, X.; Brozell, S. R.; Steinbrecher, T.; Gohlke, H.; Cai, Q.; Ye, X.; Wang, J.; Hsieh, M. J.; Cui, G.; Roe, D. R.; Mathews, D. H.; Seetin, M. G.; Sagui, C.; Babin, V.; Luchko, T.; Gusarov, S.; Kovalenko, A.; Kollman, P. A. AMBER 11. University of California San Francisco, 2010.
- Kollman, P. A.; Massova, I.; Reyes, C.; Kuhn, B.; Huo, S. H.; Chong, L.; Lee, M.; Lee, T.; Duan, Y.; Wang, W.; Donini, O.; Cieplak, P.; Srinivasan, J.; Case, D. A.; Cheatham, T. E. *Acc. Chem. Res.* **2000**, *33*, 889.
- Helge, P.; Yukihiro, I.; Takeo, H.; Thomas, S.; Juan, A.; Camacho, G.; Peter, S.; Heiko, D.; Angelika, M.; Jochen, B.; Prehn, H. M.; Eckhard, G.; Eberhard, U.; Kazuo, U. *J. Med. Chem.* **2003**, *46*, 3382.